Defect-related surface currents in InAs-based nBn infrared detectors

X. Du, B. T. Marozas, G. R. Savich, and G. W. Wicks[a)]
The Institute of Optics, University of Rochester, Rochester, New York 14627, USA

(Received 5 March 2018; accepted 21 May 2018; published online 7 June 2018)

Surface currents in mid-wave infrared photodetectors often limit the device performance. Dark current mechanisms in the bulk of a semiconductor are well understood; however, there is a poorer understanding of the mechanisms of surface currents. This work shows the existence of two types of surface current: Shockley-Read-Hall generated diffusion current and trap-assisted tunneling (TAT) through the unipolar barrier of nBn. The surface diffusion current exhibits a thermal activation energy equal to the full bandgap of InAs. Both of these surface current mechanisms are related to defects on the sidewall of the device mesa. Due to etch damage and dangling bonds, the surface defect density is typically large; thus, defect-related surface currents can be much larger than their bulk counterparts. The characteristics and temperature dependence of the surface diffusion current in two nBn structures, deep-etched (etched through the barrier layer) nBn and inverted nBn, have been shown to agree with the theory. Evidence of surface TAT current is shown in deep-etched nBn. *Published by AIP Publishing.* https://doi.org/10.1063/1.5027637

I. INTRODUCTION

III-V compound semiconductors are important materials for photon detection in the mid-wave infrared (MWIR) range of 3–μm to 5–μm wavelengths. These narrow bandgap semiconductors produce large dark currents at room temperature and usually are cooled to reduce dark currents and improve the signal to noise ratio. Demands for a less bulky and less power hungry cooling system have been a driving force to reduce the cooling requirements made necessary by the large dark currents. Dark current can be separated into two components: bulk and surface (flowing along the etched sidewall of the device mesa). Bulk dark current mechanisms in conventional photodiodes are very well understood. The bulk mechanisms are diffusion current (generated by radiative, Auger, or Shockley-Read-Hall processes), generation-recombination (G-R) current produced by Shockley-Read-Hall (SRH) generation in a depletion layer, band to band tunneling, and trap-assisted tunneling (TAT). Advanced epitaxial designs, including nBn,[1] complementary barrier infrared detector (CBIRD),[2] unipolar barrier photodiode,[3] and strained layer superlattices (SLS),[4] have been successful in suppressing many of these bulk dark currents. Among those detector types, the nBn photodetector is one of the most commonly implemented infrared detector architectures in the last decade. It consists of an n-type absorber layer, a unipolar barrier that blocks the flow of electrons while allowing holes to flow unimpeded, and an n-type contact layer. Band diagrams of conventional pn junction photodiodes and nBn photodetectors are shown in Fig. 1. Compared to the pn junction photodiode, nBn photodetectors can greatly suppress junction-related dark currents, i.e., G-R and tunneling currents, due to the unipolar barrier and the lack of depletion region.

In addition to bulk dark currents, surface current, flowing along the etched sidewalls of mesa devices, also contributes to the total dark current and often limits the performance of the detectors. Fabrication of focal plane arrays (FPAs) trends toward smaller pixels for a higher resolution and lower cost.[5] This further increases the importance of surface currents, since smaller devices are more susceptible to surface currents as they have higher surface to area ratios. The first step in suppressing surface currents is determining the physical mechanism(s) of the current. In the present work, two surface current mechanisms in InAs-based nBn detectors are identified.

InAs has a cutoff wavelength around 3.5 μm in the MWIR range and is an important absorber material for MWIR photodetectors. In pn junction device architectures, InAs-based detectors are often limited by temperature-independent surface currents, making further cooling ineffective.[6] This is caused by the well-known pinning of the surface Fermi-level in the conduction band, forming a degenerate n-type surface, regardless of the bulk material doping type.[7] The surface leakage current mechanism of InAs pn junction photodiodes is the shunt path along the sidewall produced by majority carrier drift along this n-type surface. To suppress this surface leakage mechanism, InAs nBn detectors were designed, which showed surface current suppressed to undetectable levels.[8] These first nBn detectors utilized a shallow etch processing scheme, which only etches the top contact layer and stops immediately above the barrier, shown in Fig. 2. Although this type of shallow-etched InAs nBn is very successful in suppressing surface current, it has an additional dark current problem caused by lateral diffusion current, which causes elevated dark current density, pixel-to-pixel crosstalk, and resolution degradation in image arrays. Two other nBn designs, the deep-etched nBn detector and the inverted nBn detector, prevent lateral diffusion;[9] however, they can exhibit surface current, as examined in this work. The deep-etched nBn detector is processed in the standard nBn epitaxial structure but, unlike the shallow etch processing scheme, it etches through the barrier and the

[a)]E-mail: wicks@optics.rochester.edu. Phone: 1 585 275-4867. Fax: 1 585 244-4936.

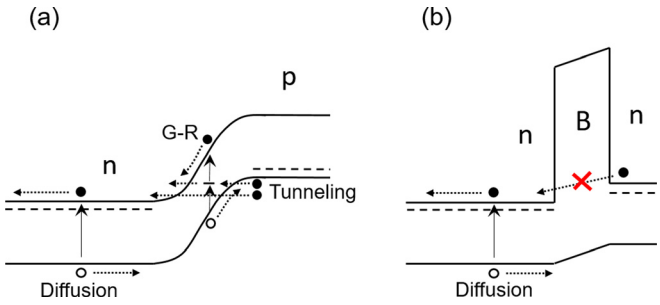

FIG. 1. Band diagram of (a) a pn junction photodiode and (b) an nBn photodetector, under a reverse bias. The pn junction photodiode is subject to junction-related dark currents, i.e., G-R, band-to-band tunneling, and TAT currents. The nBn photodetector avoids junction-related dark currents by eliminating the depletion layer of the pn junction. The unipolar barrier also blocks the flow of majority carriers, tunneling currents, and surface shunt current.

absorber. The inverted nBn structure has its absorber layer epitaxially grown above the barrier. The inverted nBn detector is subsequently processed by etching to the absorber-barrier interface without etching the barrier. Cross-sectional diagrams of these two nBn designs are also shown in Fig. 2. In the present study, the magnitude of surface current is extracted by examining the dark currents of a set of devices with different sizes. Surface current characteristics and its temperature dependence in these two nBn designs are examined. Techniques similar to those used for analyzing the bulk dark current are used for analyzing the surface current. The associated mechanisms are identified as SRH-generated diffusion current and TAT through the unipolar barrier. Understanding the mechanisms of these surface currents is important for providing guidance for future efforts to reduce them.

II. SRH GENERATION IN THE NEUTRAL REGION

It is well understood that SRH generation can occur in the depletion region of reverse-biased pn junctions, producing G-R current with half-bandgap thermal activation energies. This is a common dark current mechanism in pn junction photodiodes. SRH processes occur more generally than just in depletion layers; they can also occur in the n-type neutral absorber region; however, the magnitude and temperature dependence of SRH generation is different, as is reviewed now. In pn junction photodiodes, the neutral region SRH generation is usually not observable, because it is orders of magnitude lower than that in the depletion region. However, the ideal nBn has no depletion region and associated G-R current, which can un-mask the neutral region SRH-generated current. The SRH process has been described in the classic Shockley papers. The net rate of recombination for nonequilibrium but steady-state conditions is expressed in the following equation:[10,11]

$$U = \left(pn - n_i^2\right)/[(n + n_1)\tau_{p0} + (p + p_1)\tau_{n0}], \quad (1)$$

where n is the density of electrons in the conduction band, p is the density of holes in the valence band, n_i is the intrinsic carrier density, n_1 is the density of electrons in the conduction band when the Fermi level falls at the energy level of traps, p_1 is the density of holes in the valence band when the Fermi level falls at the energy level of traps, τ_{n0} is the lifetime for electrons injected into a highly p-type specimen, and τ_{p0} is the lifetime for holes injected into a highly n-type specimen. U is the net recombination rate, which is the difference between the actual recombination rate (pn term) and the generation rate (n_i^2 term). In the n-type absorber neutral region, $n \gg n_1$, p and p_1, and the generation rate can be reduced to

$$G = -U = n_i^2/(n \times \tau_{p0}). \quad (2)$$

The electron concentration in the absorber, n, is almost independent of temperature; therefore, the SRH generation rate is proportional to n_i^2, producing a thermal activation energy equal to full bandgap. After the minority carrier holes are generated by this SRH process, the holes flow by diffusion to produce a current with full bandgap thermal activation. The SRH generation rate and the associated current are seen to be inversely proportional to the minority carrier lifetime, which in turn is inversely proportional to the defect density. Thus, this SRH-generated diffusion current is proportional to defect density.

A previous study has identified the bulk version of this SRH-generated diffusion current. Both the full-bandgap thermal activation energy and the enhancement of dark current have been observed.[12] Rule 07 is a relation that represents the performance of state-of-the-art HgCdTe detectors. It indicates that the detectors are limited by fundamental Auger generation.[13] So far, the dark current performance of InAs-based nBn detectors has not yet reached Rule 07. It is believed that the dark current in InAs-based nBn is still limited by the SRH generation in the neutral n-type absorber region.

Due to etch damage and dangling bonds, the surface defect density is typically large, and the surface version of SRH-generated diffusion current is also expected to be large. Generally, these defect states generate minority carriers through the SRH process and can increase SRH-generated currents both in the neutral region (diffusion) and the depletion region (G-R).[14] In nBn, surface defects can create SRH

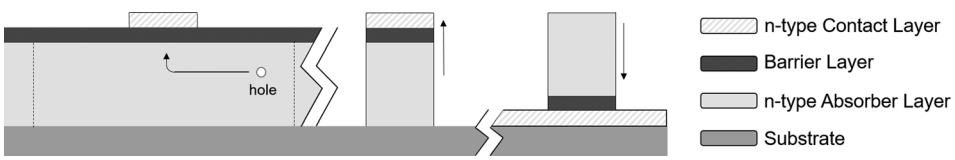

FIG. 2. Cross-sectional diagram of the epitaxial structure of shallow-etched nBn (left), deep-etched nBn (middle), and inverted nBn (right). In the shallow-etched nBn, holes can laterally diffuse and be collected, resulting in a larger collection volume (dashed lines). In the deep-etched and inverted nBn, lateral diffusion is prohibited. However, surface currents that flow along the mesa sidewalls (direction shown by the arrow) can occur.

generation, and its associated diffusion current, in regions that are neutral, i.e., not depleted, due to InAs's surface Fermi pinning in the conduction band. Such a surface current would be identified by its full-bandgap thermal activation energy and scaling with the perimeter of the mesa.

III. EXPERIMENTS AND METHODS

Standard InAs nBn and inverted InAs nBn structures were grown by Molecular Beam Epitaxy (MBE) on undoped InAs (100) substrates. Both structures had 2 μm thick unintentionally doped InAs absorbers, 0.1 μm thick unipolar barrier layers of undoped $AlAs_{0.16}Sb_{0.84}$, and 0.2 μm thick contact layers of unintentionally doped InAs. The growth order of the standard nBn structure was as follows: absorber first, then the barrier and the contact layer, while the growth of the inverted nBn structure was in the opposite order. Mesa devices were processed by standard contact photolithography, wet chemical etching, metal contact deposition of Ti/Au and a lift-off process. The solution of H_3PO_4:H_2O_2:H_2O = 1:1:1 was used for InAs etch and HCl:H_2O_2:H_2O = 1:1:9 for barrier etch. Both etchants provide large selectivity between InAs and the barrier. Three types of devices were fabricated: shallow-etched standard nBn, deep-etched standard nBn and inverted nBn. No surface passivation was performed. All fabricated devices were measured using a Lakeshore cryogenic probe station for their temperature-dependent dark current I-V characteristics. The measurements were carried out using either an HP 4155B or a Keithley 4200 A parameter analyzer.

The conventional way of assessing whether currents are bulk or surface currents is by plotting I/A versus P/A for various size devices. I is the measured dark current for a device, A is the mesa area and P is the perimeter of the device mesa. The relationship between I/A and P/A is described by the following equation:

$$I/A = J_{surface} \times P/A + J_{bulk}, \quad (3)$$

where $J_{surface}$ and J_{bulk} are the surface current density [A/cm] and the bulk current density [A/cm^2], respectively. This analysis is not completely applicable to early nBn detectors fabricated by the shallow etch process due to the complicating presence of lateral diffusion current. In this study, this technique can be applied to deep-etched and inverted nBn designs as the lateral diffusion is eliminated in these device architectures.

IV. RESULTS AND DISCUSSION

I/A versus P/A plots of both deep-etched nBn devices and inverted nBn devices at 254 K are shown in Fig. 3. Current density values of different devices are taken at a reverse bias of −0.4V. This bias is chosen as a larger value than the turn-on voltage of the deep-etched nBn. The turn-on voltage of the deep-etched nBn is around −0.25V, as shown below. This turn-on voltage of the dark current is comparable to the turn-on voltage observed in the photoresponse. The turn-on voltage of the inverted nBn is less clear, possibly due to an additional valence band barrier. However, the same bias of −0.4 V is chosen. Clear slopes for both types of

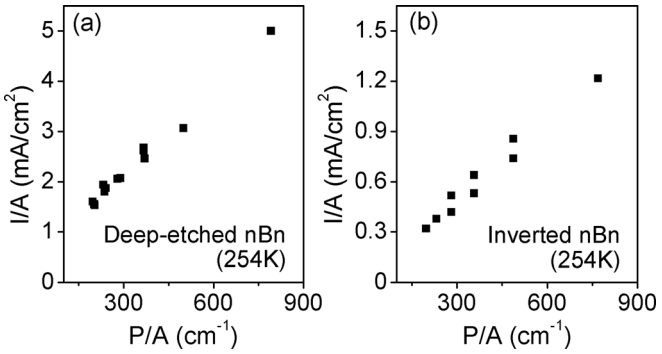

FIG. 3. Current/area ratio at a reverse bias of −0.4 V versus perimeter/area ratio at T = 254 K for (a) deep-etched nBn devices and (b) inverted nBn devices. The device mesa size ranges from 60 μm × 60 μm to 210 μm × 210 μm. The slope of a linear fit to the data is proportional to the surface current density. Devices with negligible surface current would produce graphs that are horizontal lines. The graphs of these devices exhibit significant slopes, indicating the presence of substantial surface currents.

devices are observed in Fig. 3, indicating the presence of surface currents in both types of devices. Upon fitting the data points, deep-etched devices show surface current at the level of 5.2×10^{-6} A/cm and inverted devices show surface current at the level of 1.6×10^{-6} A/cm at 254 K.

The observable surface currents (slopes) in this I/A versus P/A analysis mean that the carrier generation rate at the surface is higher than that in the bulk, hence producing a higher dark current density in a smaller device. In addition, due to the sensitivity of this analysis, if devices are surface current limited, the y-intercept would be very sensitive to device-to-device variation and has large uncertainty. In this study, due to the above reason, only $J_{surface}$ is taken into account. This same analysis was performed at other temperatures to acquire the temperature dependence of the surface component for both types of devices. An Arrhenius plot of the surface current density, $J_{surface}$, at a reverse bias of −0.4 V is shown in Fig. 4 for both types of devices. For the deep-etched and inverted nBn devices, the thermal activation energy of $J_{surface}$ around room temperature is calculated to be 0.37 eV and 0.36 eV, respectively, close to the full bandgap

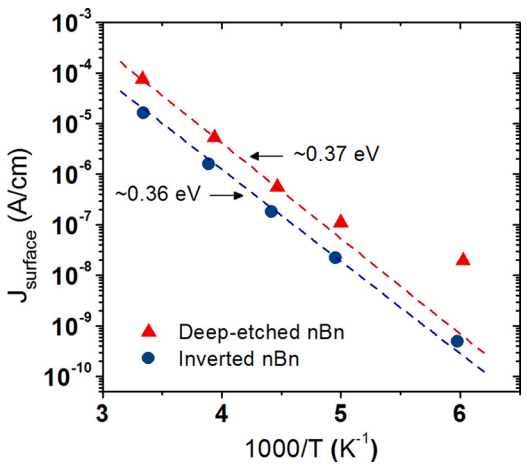

FIG. 4. Arrhenius plot of surface current density, $J_{surface}$, at a reverse bias of −0.4 V for deep-etched and inverted nBn. Thermal activation energy of the surface current at room temperature is 0.37 eV for deep-etched nBn and 0.36 eV for inverted nBn.

of InAs at room temperature, which indicates a diffusion limited characteristic, and its perimeter dependence indicates that it is surface current.

The characteristics of higher generation rate at the surface and full-bandgap thermal activation energy of the surface current are consistent with the theory of diffusion current produced by SRH generation in the neutral region along the mesa sidewalls. Etching through the absorber material creates a high defect density at the exposed absorber sidewalls and a surface n-type SRH (full bandgap activation energy) generation occurs. The resulting electrons flow away from the barrier and exit the device; while the resulting holes flow across the barrier to exit the device at the opposite contact. This surface current mechanism dominates near room temperature.

Trap states in the electron barrier can introduce TAT current.[15] TAT current in deep-etched nBn has been identified in the previous study.[9] It is identified by a temperature-independent characteristic in the device I-V-T curves, shown in Fig. 5. The surface current Arrhenius plot of deep-etched nBn also shows an indication of lowered thermal activation energy as the temperature cools down, as indicated in Fig. 4, suggesting this TAT current may occur at the surface. The assignment of this TAT current as a surface current is further supported by a comparison with the same size shallow-etched device that is processed using the same wafer, shown in Fig. 6. The deep-etched (etched through the barrier) devices show substantially higher dark current than the shallow-etched (no barrier etch) device at lower temperatures. Neither the shallow-etched nBn (no barrier etch) nor the inverted nBn without the barrier etch shows TAT current. Since TAT is only observed in the deep-etched devices (etched through the barrier), it is clear that the introduced trap states along the barrier sidewall during the barrier etch creates the TAT, thus the TAT must be a surface current.

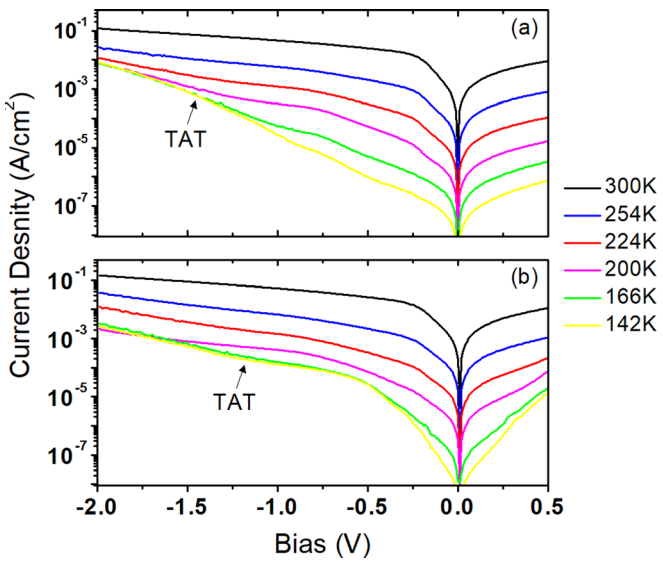

FIG. 5. Temperature-dependent dark current characteristics of two 180 μm $\times$ 180 μm deep-etched nBn devices. Both devices show turn-on voltages of ~0.25 V. The temperature-independent surface TAT current is indicated in the figure. There is significant device-to-device variation: device in (b) shows a higher level of surface TAT at a lower bias than the device in (a).

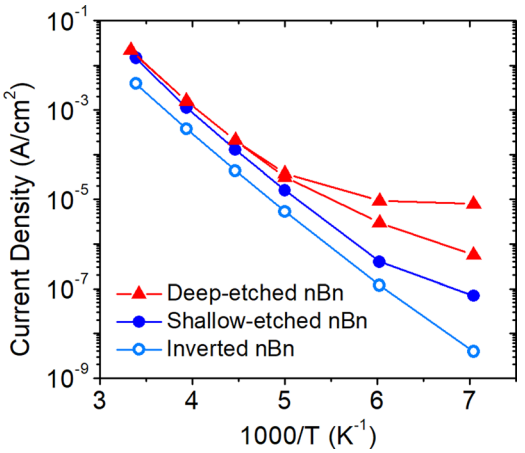

FIG. 6. Arrhenius plot of current density at a reverse bias of −0.4 V for two deep-etched nBn devices, a shallow-etched nBn device and an inverted nBn device. All devices are of 180 μm $\times$ 180 μm. Deep-etched nBn devices show substantially higher dark current and lower thermal activation energy than the shallow-etched device at lower temperatures due to the surface TAT. Inverted nBn device is not subject to surface TAT and shows full-bandgap thermal activation energy at all temperatures.

These traps help electrons tunnel through the barrier. The trap density can have a large variation between devices, resulting in different levels of surface TAT, supported in Figs. 5 and 6. Avoiding etching through the barrier is an effective way of avoiding surface TAT current. Rearranging the growth order and avoiding the barrier etch may be helpful, as in the inverted nBn structure.

V. CONCLUSION

Shockley-Read-Hall generation through defect levels in the neutral region of nBn devices creates diffusion dark current with full-bandgap thermal activation energy. The high defect density at the surface can greatly enhance this process, producing surface currents with full-bandgap thermal activation energy. The deep-etched and inverted nBn have both been found to have this type of surface current, a higher generation rate at the surface, and full-bandgap thermal activation energy. It is attributed to this surface SRH process at exposed absorber sidewalls. This process can also generally exist in other types of detectors with exposed absorber sidewalls. TAT current can also occur in the case of high trap density on the sidewalls of the electron barrier. A barrier etch can introduce such traps at the barrier sidewalls and generate surface TAT current. Rearranging the growth order and avoiding the barrier etch can help with limiting the surface TAT current.

ACKNOWLEDGMENTS

This work was supported by Army Research Office.

[1]S. Maimon and G. W. Wicks, Appl. Phys. Lett. **89**, 151109 (2006).
[2]D. Z. Y. Ting, C. J. Hill, A. Soibel, S. A. Keo, J. M. Mumolo, J. Nguyen, and S. D. Gunapala, Appl. Phys. Lett. **95**, 023508 (2009).
[3]G. R. Savich, J. R. Pedrazzani, D. E. Sidor, S. Maimon, and G. W. Wicks, Appl. Phys. Lett. **99**, 121112 (2011).
[4]D. L. Smith and C. Mailhiot, J. Appl. Phys. **62**, 2545 (1987).
[5]A. Rogalski, P. Martyniuk, and M. Kopytko, Rep. Prog. Phys. **79**, 046501 (2016).

[6]D. E. Sidor, G. R. Savich, and G. W. Wicks, Proc. SPIE **9616**, 96160U (2015).
[7]S. Tiwari and D. J. Frank, Appl. Phys. Lett. **60**, 630 (1992).
[8]J. R. Pedrazzani, S. Maimon, and G. W. Wicks, Electron. Lett. **44**, 1487 (2008).
[9]X. Du, G. R. Savich, B. T. Marozas, and G. W. Wicks, J. Electron. Mater. **47**, 1038 (2018).
[10]W. Shockley and W. T. Read, Jr., Phys. Rev. **87**, 835 (1952).
[11]C. T. Sah, R. N. Noyce, and W. Shockley, Proc. IRE **45**, 1228 (1957).
[12]G. R. Savich, D. E. Sidor, X. Du, C. P. Morath, V. M. Cowan, and G. W. Wicks, Appl. Phys. Lett. **106**, 173505 (2015).
[13]W. E. Tennant, J. Electron. Mater. **39**, 1030 (2010).
[14]A. Rogalski, *Infrared Detectors*, 2nd ed. (CRC Press, 2010), p. 210.
[15]A. Soibel, S. B. Rafol, A. Khoshakhlagh, J. Nguyen, L. Hoglund, A. M. Fisher, S. A. Keo, D. Z. Y. Ting, and S. D. Gunapala, Appl. Phys. Lett. **107**, 261102 (2015).